Accepted Manuscript

Monotonic and cyclic behaviour of cast and cast-forged AZ80 Mg

A. Gryguc, S.K. Shaha, S.B. Behravesh, H. Jahed, M. Wells, B. Williams, X. Su

PII: S0142-1123(17)30288-8
DOI: http://dx.doi.org/10.1016/j.ijfatigue.2017.06.038
Reference: JIJF 4394

To appear in: *International Journal of Fatigue*

Received Date: 1 December 2016
Revised Date: 21 June 2017
Accepted Date: 28 June 2017

Please cite this article as: Gryguc, A., Shaha, S.K., Behravesh, S.B., Jahed, H., Wells, M., Williams, B., Su, X., Monotonic and cyclic behaviour of cast and cast-forged AZ80 Mg, *International Journal of Fatigue* (2017), doi: http://dx.doi.org/10.1016/j.ijfatigue.2017.06.038

Monotonic and cyclic behaviour of cast and cast-forged AZ80 Mg

A. Gryguc [1], S.K. Shaha[1], S.B. Behravesh[1], H. Jahed [1], M. Wells [1], B. Williams[2], X. Su[3]

[1]Department of Mechanical & Mechatronics Engineering, University of Waterloo, 200 University Avenue West, Waterloo, ON N2L 3G1, Canada
[2]CanmetMATERIALS, Natural Resources Canada, 183 Longwood Road South, Hamilton, ON L8P 0A1, Canada
[3]Ford Research and Innovation Center, 2101 Village Road, Dearborn, MI 48124, USA

ABSTRACT

Tensile and strain-controlled fatigue tests were performed to investigate the influence of forging on the performance of cast AZ80 magnesium alloy. The obtained microstructural analysis showed that the as-cast AZ80 magnesium alloy has dendritic α-Mg phase with eutectic $Mg_{17}Al_{12}$ morphology and a random texture. In contrast, the forged samples showed refined grains and a strong basal texture. During tensile testing, a maximum yield and ultimate tensile strength of 182 MPa and 312 MPa were obtained for the forged samples, representing increases of 121% and 33%, respectively, from the as-cast condition. At the same time, a significant improvement (73%) in ductility was obtained in forged samples. It was also observed that the forged samples achieved comparatively longer fatigue life under strain-controlled cyclic loading. Analysis of the fracture surfaces showed that a cleavage-type morphology was typical for the as-cast samples, while the occurrence of dimples and other evidence of plastic deformation were identified in the fracture surfaces of the forged specimens, indicating a more ductile response. Forging caused grain refinement and texture modification, both of which enhance alloy performance by improving strength and ductility, and leading to longer fatigue life. Strain and energy-based models were investigated for their suitability to predict the life of the forged material. Both the Smith-Watson Topper and the Jahed-Varvani energy-based models gave reliable life prediction.

Keywords: AZ80, Forging, Texture, Fatigue Characterization, Fracture, Fatigue Modeling.

1. Introduction

There has been a growing strong impetus to increase fuel efficiency and decrease emissions in the automotive industry over the past several decades. Implementation of lightweight materials in structural applications are at the forefront of this effort, as this strategy can improve vehicle efficiency, longevity, and performance. The multi material lightweight vehicle (MMLV) is an emerging philosophy, and includes extensive use of lightweight materials for structural components. Importantly, this philosophy dictates that their location in the vehicle be determined directly by the location of their optimal performance. Magnesium (Mg) and its alloys have significant promise in this area, with widespread applicability in fatigue-critical components, such as suspension control arms, since they are the lightest commercially available structural metal and their cyclic properties are similar to those of the heavier, more conventional materials used in industry [1]. However, the inferior cast properties and poor formability of Mg alloys at room temperature, resulting from strong crystallographic texture, and consequential anisotropic mechanical properties commonly formed during processing, limits the application of Mg alloys for manufacturing of complex parts such as a control arm. Forging is a near net-shape manufacturing technique that offers significant benefits as a material processing technique to produce a heavily refined wrought microstructure, lower internal defect density, and recrystallized grain structure, resulting in superior strength, improved ductility, and longer fatigue life [2]. The focus of the

present study is to examine the effect of forging, as an alternative for manufacturing complex Mg parts, on the monotonic and fatigue behavior of Mg.

The AZ80 alloy is a Mg alloy with good forgeability, a high aluminium content, and superior strength. The majority of published literature on AZ80 mechanical properties has focused on the static and fatigue properties of extrusion [3]–[14] cast [15]–[17][8] and plate [18] AZ80 Mg. Several researchers have investigated the fatigue behaviour of as-cast and wrought (extrusion, rolled plate/sheet) AZ80 Mg in stress-controlled [3]–[5], [8]–[12], [19]–[22], strain-controlled [12][13][18][23], and fatigue crack growth rate [5], [9], [24], [25] testing.. Zhou et al. [16] investigated the hot workability characteristics of as-cast AZ80 Mg and found that at temperatures below 300°C and strain rates of 10^{-2} s^{-1}, flow localization bands limit the materials ductility, making it difficult to deform. They also studied the dynamic recrystallization (DRX) behaviour and found that it occurred over a temperature range of 425°C–500°C. Quan et al. [17] investigated the hot deformation characteristics of cast-homogenized AZ80 at 350°C and found a decrease in average grain size with an increase in strain rate. The observed average grain size of the cast material was 240 μm. Following deformation, (total height reduction of 60%) at 350°C, the grain size was refined to 120, 110, 94, and 50 μm under stain rates of 0.01, 0.1, 1, 10 s^{-1}, respectively. Nový et al. [8] investigated both the static and very high-cycle fatigue (VHCF) properties using ultrasonic push-pull stress-controlled testing. In as-cast AZ80, they observed a yield and ultimate strength of 107 and 130 MPa, respectively. They found ductility to be very limited with a failure elongation of only 2%, and prominent intermetallic content with sizes ranging from 5–20 μm. They also observed that only surface-induced cracks occurred in AZ80 under cyclic loading, with no observed endurance limit. They also discussed the finding that primary fatigue crack initiation sites are governed by microscopic defects such as pores, inclusions, or intermetallics in the low-cycle fatigue (LCF) to high-cycle fatigue (HCF). In contrast, they observed that in the VHCF, fatigue crack initiation is mostly controlled by the properties of the matrix, while the role of microscopic defects is minimal. Shiozawa et al. [12] performed LCF strain-controlled tension-compression fatigue tests on Mg extrusion AZ31, AZ61, AZ80;AZ80 had superior fatigue properties relative to the other alloys [26]. They also observed that in strain-controlled fatigue testing, a tensile mean stress was developed, caused by the tension/compression yield asymmetry typical of textured Mg alloys and the resulting twinning-detwinning cyclic deformation mechanism. They utilized a total strain energy density-based model, first developed for rolled AZ31 by Park et al. [27] as a modification to the well-known Morrow model, to reliably predict the fatigue life of extruded AZ80 Mg alloy. More recently, Wang et al. [23] utilized this modified Morrow model to successfully predict the LCF life of extruded AZ80 using a total strain energy density-based approach.

Many researchers have focused on the high temperature deformation behaviour of forged AZ80 [4] [6][7][15]–[17][20][22][28]–[37]. However, studies that discuss the effect of thermomechanical history resulting from the forging process on the tensile/compressive and fatigue properties of AZ80 after forging are limited. Kobold et al. [28] performed both axial and radial open die forging of extruded AZ80-T5 at rates of 5–20 mm s^{-1}, and observed no significant differences in the anisotropy of the material flow regardless of the forging direction. Furthermore, they concluded that the optimal isothermal forging temperature was 350°C, and that the optimum condition tends toward lower temperatures and higher strain rates. Kurz et al. [6] observed in die-forged AZ80-F that increasing the forging temperature decreases the mechanical strength, but enhances ductility as a result of an increase in grain size and more homogeneous microstructure. They also concluded that at higher deformation rates (300–400 mm s^{-1}), lower forging temperatures (240°C) are desirable. Rivers et al. [22] investigated the stress-controlled fatigue of samples machined from a forged AZ80 automotive wheel and observed an fatigue strength of approximately 98 MPa. The effect of the forging process on the strength, ductility, and strain-controlled fatigue behaviour of AZ80 has yet to be investigated in detail.

In this study, the effect of forging parameters on the tensile/compressive and forging on fatigue behavior of AZ80 was examined in detail and compared with the as-cast condition. A texture and microstructural link between the mechanical behavior of as-cast and forged AZ80 was established. The effect of material orientation on the tensile and compressive behavior of AZ80 is also discussed. Results from a complete fully reversed fatigue test results spanning from LCF to HCF are presented. Coffin-Manson and energy-based fatigue properties of as-cast and forged AZ80 were obtained, and the suitability of energy-based fatigue parameter in predicting the life of AZ80 was examined.

2. Material and Experiments

The material used in this investigation was commercially-available AZ80 Mg alloy (8.0 ±0.2% Al content, with other elements composition as per ASTM B91-12 standard). The material was received from Magnesium Elektron North America Inc. in the form of an as-cast billet with a diameter of 300 mm and a length of 500 mm in the as-fabricated condition. The forging of the material was conducted at CanmetMATERIALS (Hamilton, Canada) using billets (⌀ 63.5 mm, 65-mm long), which were machined from the 300-mm diameter AZ80 casting at a position of 70% of the radius. All forging trails were carried out on a 500-ton hydraulic press with an upper and lower platen (die), which were both flat. Two forging temperatures (350 and 450°C) were examined. The billet and tooling were heated separately to the same temperature. The orientation of the billet to the press was such that the radial direction was along the direction of the press stroke (i.e. direction of forging was coincident to the radial direction of the billet). Forging was carried out at two different displacement rates (39 and 390 mm/min), which fall within the slower regime of die forgings presented by Kevorkijan et al. [37]; however the approximate average strain rates presented in this study lie between those presented by Kevorkijan et al. [37] and Kurz [6]. For the quasi-static study, three forging conditions investigated in this study will subsequently be referred to as S1 (350°C and 39 mm min^{-1}), S2 (450°C and 39 mm min^{-1}), and S3 (450°C and 390 mm min^{-1}). The cast and machined billets were forged to a height of 13 mm, then air cooled. Graphite lubricant was used to coat the surface of every billet prior to forging. Although the die temperature remained almost constant throughout the test, heat loss to the surrounding air during forging was expected for the billet, particularly for the slower forging rate condition. Figure 1(a) and (b) show the orientation for which the metallographic, tensile, and fatigue-tested specimens were extracted from both the cast and forged billets. LD, RD, TD, and FD represent longitudinal, radial, transverse, and forging directions, respectively. All specimens were extracted from a point located at 75% of the radius of the as-cast billet. All specimens extracted from the forged billets had axes oriented in the longitudinal direction.

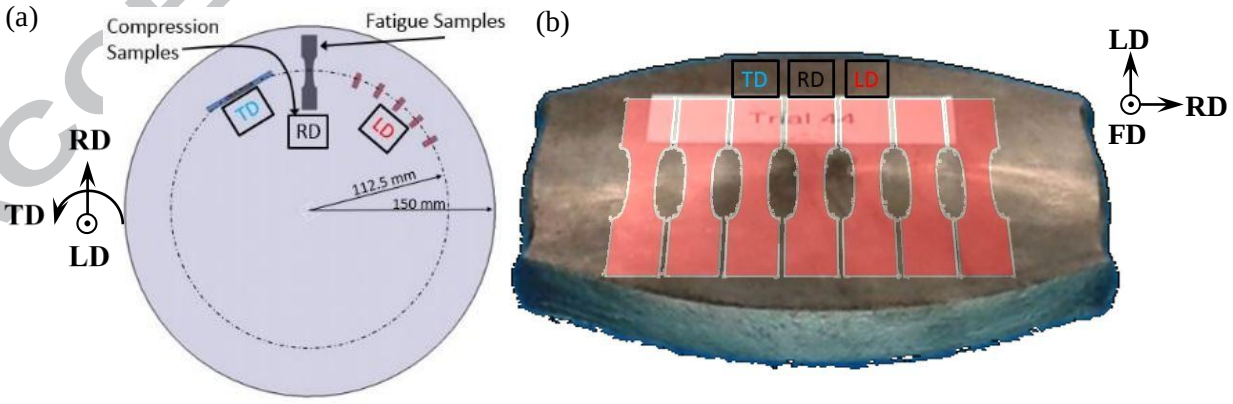

Figure 1 - Schematic image showing tensile/fatigue and compression sample extraction from (a) the as-cast billet, (b) the sample forged at 39 mm min^{-1} and 350°C

The metallographic samples were prepared following the metallographic techniques outlined in ASTM E3-11 with acetic-picral etchant similar to that used by Roostaei et al. [38]. The microstructure was observed using a light optical microscope (LOM) and a scanning electron microscope (SEM), coupled with energy-dispersive X-ray spectroscopy (EDS). The average grain intercept method is used to quantify the grain size. The texture measurements were performed on polished samples using a Bruker D8-Discover equipped with a VÅNTEC-500 area detector, with a radius of 135 mm and using Cu-Kα radiation at 40kV and 40 mA. During the measurement, the incident beam and the detector were placed at a fixed 2θ angle of 40°. The collimator size was 1.0 mm. The sample was mounted on the motorized stage, which was oscillated at an amplitude of 1.5 and 2.5 mm, and a speed of 3.5 mm s^{-1} and 5.5 mm s^{-1} for the *X* and *Y* axis, respectively. The samples were tilted between 0 and 75°, with a step of 15° considered as the *Ψ*-scan, while the sample rotation, known as *Φ*-scan, was between 0 and 360°, with a step size of 5°. The sample was scanned for 20 s at each orientation. The Debye–Scherrer diffraction rings were collected using the area detector in a 2-D diffraction image. Then, the incomplete pole figures for the {0002}, $\{10\bar{1}0\}$, $\{10\bar{1}1\}$, and $\{1\bar{1}02\}$ planes were extracted from the diffraction rings. The complete pole figures were then calculated using the DIFFRAC.Suite: Texture software.

Tensile test samples with geometries according to Roostaei et al. [38] were extracted from the as-cast billet and flatbread shape forged samples as shown in Figure 1 (a),(b). The thickness of the samples extracted from the as-cast billet was 4 mm, and from the forged billet was 6 mm. The quasi-static tensile tests were performed according to ASTM standard E8/E8M-15a using an 8874 Instron Servo-Hydraulic test machine operating in displacement control mode. Compressive test samples of cuboid geometry with side lengths of 7.6 mm were extracted as shown in Figure 1(a) and (b). The quasi-static compressive tests were performed using a MTS 810 Servo-Hydraulic test machine operating in displacement control mode. For both compressive and tensile monotonic tests, the displacement rate of the crosshead was 1 mm min^{-1}. Strain measurement was accomplished using a GOM ARAMIS 3D 5MP DIC system. The average strain rate within the gauge section of measurement for both tests were 1.4E−3 sec^{-1}.

The fatigue tests were performed as per ASTM E606 in an ambient environment using a MTS 810 Servo-Hydraulic test machine operating in strain control mode at a frequency range of 0.25–2 Hz. Strain was measured and controlled using a MTS 632.26 extensometer with a 6-mm gauge and travel of ± 1.2-mm, until stabilization of the cyclic hysteresis loop was achieved; for HCF tests with elastic response, the test was switched to force control mode, and the frequency was increased to 30 Hz. The tests were conducted at a zero mean strain (i.e., $R_L = -1$, fully reversed strain cycle) and strain amplitudes of between 0.1% and 1.4%. Failure criteria for the test was considered to be a 50% drop in peak load during strain control mode or final rupture of the specimen gauge section in force-control mode. The fracture surfaces after tensile and fatigue tests were examined using SEM techniques (JEOL JSM-6610LV SEM equipped with AZ-TEC EDS).

3. Results and Discussion

3.1 Microstructure and Texture

As depicted in Figure 2(a) and (c), the as-cast sample was found to consist of primarily α-phase, in which aluminium-rich β-phase ($Mg_{17}Al_{12}$) is precipitated along the grain boundaries. This agrees with the microstructure of as-cast AZ80 observed by Nový et al. [8], the grain morphology of which was similar to that observed here, while the average grain size (80–140 μm) was slightly more refined than that observed

in this study. The forged conditions S1, S2, and S3 (Figure 2(b), (d), (e)–(h)) all exhibit a recrystallized microstructure with fairly homogeneous grain morphology, albeit "pancake"-like in nature. For all forged conditions, the precipitate morphology observed at higher magnifications have a discontinuous intergranular structure, which is similar to that observed by Lai et al. [39] in extruded AZ80 that was aged at 300°C for 1 hr, which is comparable to the thermal history experienced in the forged samples presented in this study. The average grain size for the forged conditions ranged from 14.1–34.4 μm, with condition S1 (Figure 2(b)) having the most refined microstructure. As the forging temperature and rate increase, the observed average grain size also increases (Figure 3).

Figure 2 illustrates the as-cast and forged conditions S1 ((b), (d)), S2 ((e), (g)), and S3 ((f), (h). The as-cast condition (Figure 2 (c)) exhibits randomized basal (0002) and prismatic $(10\bar{1}0)$ texture. All forged conditions (Figure 2 (d), (g) and (h)) exhibit strong basal texture. Based on the basal pole figures, it is clear that the c-axis orientation of the forged material is coincident with the forging direction; similar reorientation of the c-axis due to forging has been reported by several researchers [40]–[42]. Previous work by Gryguc et al. [43] on axially and radially forged AZ31B extruded billets show an analogous c-axis reorientation in extruded AZ31 following forging. The effect of forging on the initial random texture is a local reorientation of newly recrystallized grains, causing their crystal axis to align with the forging axis as the deformation progresses. This causes the basal texture strengthening to be planar in nature for all forged conditions. Wang et al. [44] found that in both extruded and sheet AZ31 Mg, following significant plastic strain, most c-axis orientations, which are favourable for twinning, will re-orient themselves to the direction of forging; this directly supports the findings presented here. The texture intensity in the forged material is inversely correlated to temperature, with very weak sensitivity to forging rate. The changes in grain size and basal pole figure intensity as a function of forging condition are depicted in Figure 3. The highest basal intensity and lowest grain size were achieved at the lower temperature (350°C) and forging rate (39 mm min^{-1}). An increase in temperature had the effect of decreasing texture intensity and increasing average grain size. This observation agrees with earlier findings of several other researchers [35][33][45].

Many researchers have investigated the effects of processing parameters on the mechanical properties of AZ80 using simple compressive upset testing using Gleeble thermomechanical testing equipment. Quan et al. [17] investigated the effect that strain rate had on cast AZ80 at 350°C. They found that with a total height reduction of 60% (lower than the 80% height reduction considered in this study), grain refinement is more pronounced at higher strain rates as a result of more vigorous DRX behaviour. Liu et al. [46] presented similar findings for cast AZ91 Mg at various temperatures (250–450°C); they revealed that the effect of increasing strain rate was an increase in grain refinement, while an increase in temperature caused grain growth and improved microstructure homogeneity. Lou et al. [26] presented analogous results when investigating the effects of strain rate on extruded AZ80 at temperatures ranging from 250–450°C, both of which support the finding of this study that lower temperature forging conditions results in more refined microstructure (Figure 2). However, other researchers have observed that an increase in strain rate resulted in more vigorous grain refinement on their temperature-controlled Gleeble specimens, which were water quenched following testing [17][26][46]. These results differ from those presented here (Table 1, Figure 2) as condition S3 (390 mm min^{-1}) has an average grain size that is ~13 μm larger than condition S2 (39 mm min^{-1}). This can be attributed to the fact that during forging, only the die temperature and initial billet temperature were controlled, unlike the conditions of the Gleeble tests, in which the billet temperature is controlled throughout deformation. Since the heat of deformation is greater for the higher rate forging, the temperature rise due to deformation in condition S3 would be larger than that in S2, potentially causing the observed grain growth. Additionally, following deformation, the forgings were left to air-cool, unlike the water quenching following the Gleeble tests.

Finally, this difference can be attributed to the difference between the style of forging during a Gleeble test (axial upset of small cylindrical sample) and this study (radially upset bulk forging). The lower temperature forging condition S1 is considered to produce the best microstructure of all three samples, based on the more refined and recrystallized morphology it possesses. At the higher temperature (450°C) forgings (S2 and S3), microstructure homogeneity further improved, and was coupled with grain growth and apparent refinement in β-phase morphology.

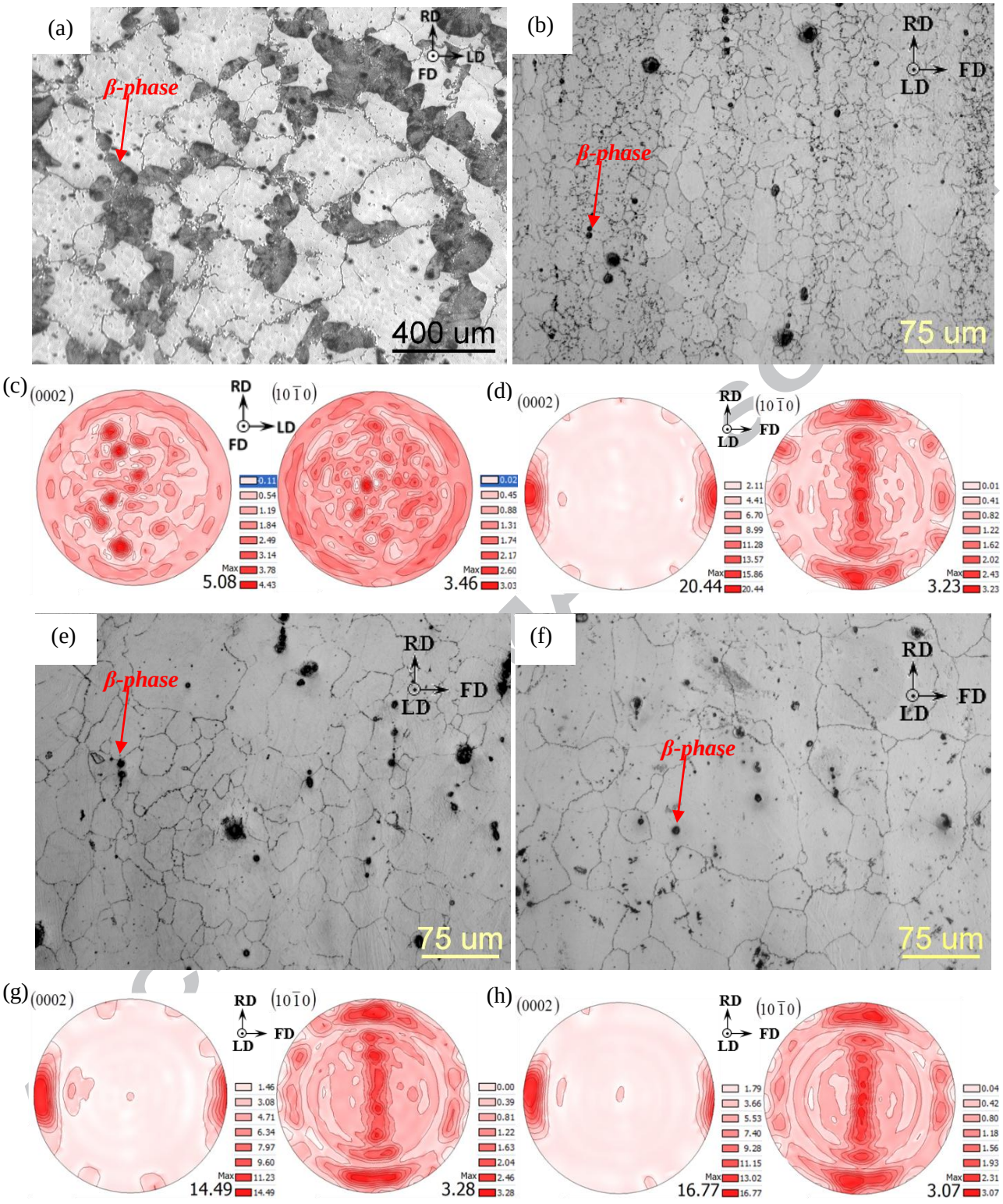

Figure 2 - Typical LOM microstructure and XRD pole figures for As-Cast ((a) and (c)), forged condition S1 ((b) and (d), forged condition S2 ((e) and (g)), and forged condition S3 ((f) and (h))

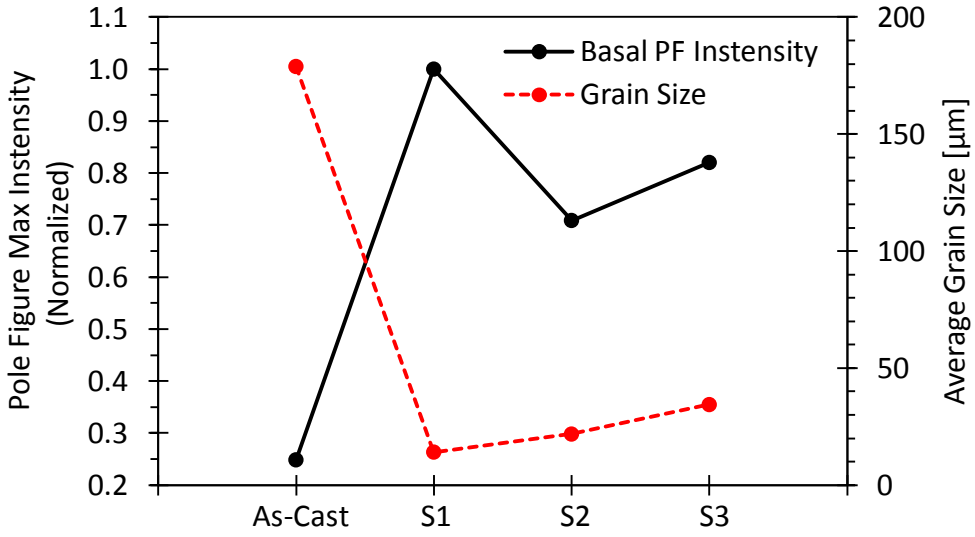

Figure 3 - Relationship between basal pole figure max intensity and average grain size for as-cast and forged conditions (S1, S2, and S3)

3.2 Monotonic and Cyclic

Table 1 summarizes the test results of the investigated samples. Figure 4(a) and Figure 5(a) show the engineering stress-strain response in tension (Figure 4(a)) and compression (Figure 5(a)) for the as-cast and forged (S1, S2, and S3) materials in the longitudinal direction.

Table 1- The relationship between microstructural, monotonic, and cyclic properties of as-cast and forged AZ80-F Mg alloy. Tensile properties are presented first, followed by compressive properties in parenthesis.

ID	Forging rates (mm/min)	Forging Temperature (°C)	Grain size (µm)	σ_{YS} (MPa)		ε_{Fail} (%)	σ_{ULT} (MPa)
				Monotonic	Cyclic		
Cast	As-Cast	-	178.9±67	82.2 (93.8)	147.0 (153.5)	8.5 (15.3)	234.1 (318.2)
S1	39	350	14.1±0.7	173.8 (124.5)	258.3 (145.4)	14.1 (8.5)	311.9 (373.0)
S2	39	450	21.8±2.4	176.9 (111.2)		15.8 (9.6)	310.6 (366.7)
S3	390		34.4±2.7	181.7 (69.2)		14.2 (8.3)	306.1(325.9)

It can be seen that the yield, ultimate strength, and, in some cases, the fracture strain substantially increase following forging. In general, substantial increases in tensile yield stress and fracture strain were observed in the material after forging. This was coupled with a moderate increase in compressive yield strength, tensile ultimate strength, and compressive ultimate strength after forging. However, the fracture strain in compression decreased to some degree in all of the forging conditions. The increase in mechanical properties of as-forged compared to as-cast condition is attributed to the grain refinement and texture intensification that arises from the reorientation of the randomized c-axis orientation in the as-cast material in the direction of deformation once forged. All forging conditions have very similar monotonic yield/ultimate strengths and hardening behaviours under tension. At the higher temperature (450°C) forgings (S2 and S3) a reduction in compressive yield and ultimate strength was observed, but the tensile strength remained similar to all other forged conditions. This trend partially agrees with findings presented by Kurz et al. [6] for AZ80 die forgings, who also reported a decrease in tensile strength at higher temperatures.

Figure 4(b) and Figure 5(b) show a comparison of the cyclic vs. monotonic stress-strain curves for both the as-cast and forged material in tension (Figure 4(b)) and compression (Figure 5(b)). The cyclic tension and compression stress-strain curves were constructed from the peak and valley stresses for the stabilized cycle during fatigue testing for each respective strain amplitude. Stabilized cycle is the cycle at 50% of the number of cycles to failure. In general, data from the forged conditions S1, S2, and S3 follow the same cyclic tensile stress-strain curve. For this reason the fatigue results of the three conditions will be presented collectively.

The compressive stress-strain curves shown in Figure 5(a) illustrate evidence of mixed hardening in the as-cast condition and purely sigmoidal hardening behaviour for all forged conditions. As expected from the random texture shown in Figure 2(c), the as-cast material exhibited nearly symmetric yield strength in tension and compression, with slip and diffused twinning being dominant in both directions. In contrast, the forged material exhibits a very asymmetric yielding response, with the degree of asymmetry increasing as both temperature and forging rate increase (Figure 6a). Based upon the hardening responses seen in forged conditions S1, S2, and S3, and the strong basal texture shown in Figure 2(d), (g), and (h) the deformation mechanism in tension is dominated by basal slip (as the direction of loading is parallel to the basal plane), and the deformation in compression is dominated by twinning (extension twinning activated via extension along the c-axis). This sigmoidal behaviour, characterized by three distinct hardening stages, has been discussed by other researchers [49][43].

Under cyclic loading, the as-cast and all 3 forged conditions show cyclic hardening, where the increase in peak and valley stresses is relative to those of the monotonic results. As seen in Figure 4 and Figure 5, the as-cast material exhibits very similar cyclic hardening in tension and compression, with the peak stresses observed in the stabilized cyclic response being 73 MPa higher than those observed in the monotonic response at and beyond strain amplitudes of 0.9%. The forged material however, shows more pronounced cyclic hardening in tension, with the highest degree of hardening occurring at a strain amplitude of 1.1%, corresponding to an increase of 80 MPa in peak (tensile) stress and 58 MPa in valley (compressive) stress relative to the monotonic response. Figure 6(b) illustrates the change in yield strengths following cyclic hardening for both the as-cast and forged material. There is an increase of 62 MPa in the yield strength of the cast material in tension and compression, and asymmetric increases of 81 MPa in tension, and 34 MPa in compression for the forged material. The asymmetric hardening responses of conditions S1, S2, and S3 is attributed to the differences in the deformation mechanism in tension and compression reversals, induced by the texture intensification via forging.

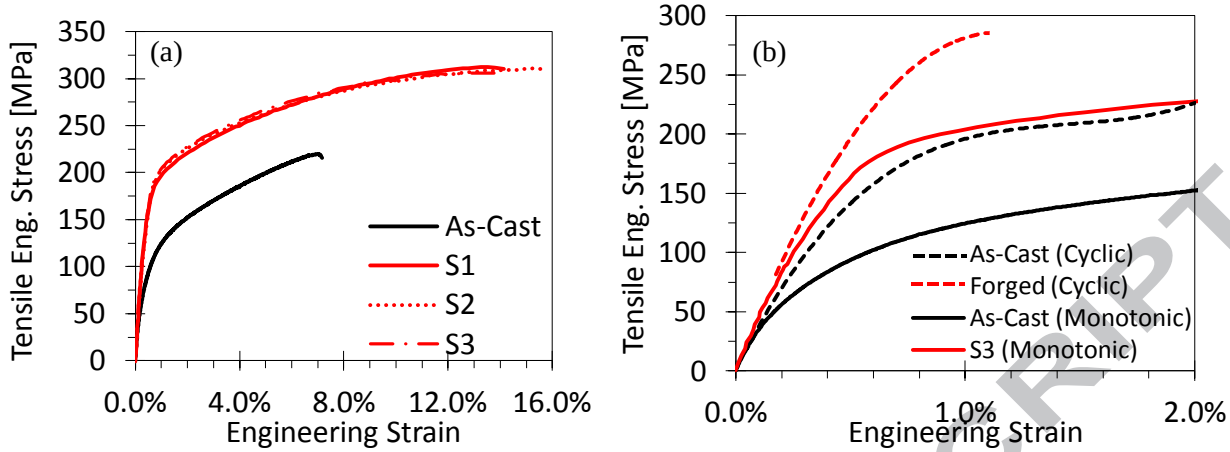

Figure 4 – Tensile (a) monotonic and (b) cyclic stress-strain curves for as-cast (black) and forged Mg (red)

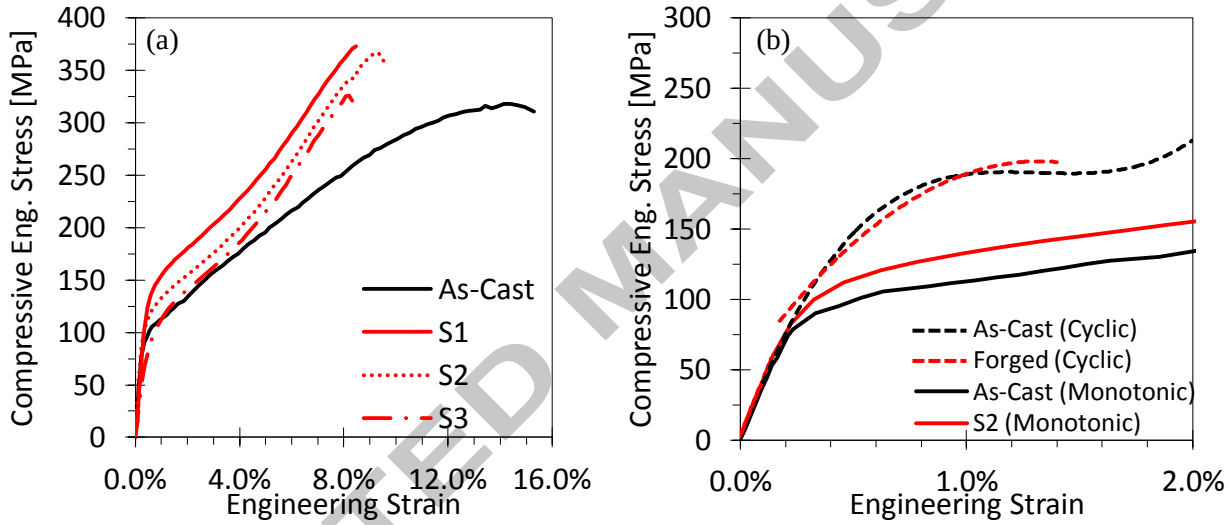

Figure 5 – Compressive (a) monotonic and (b) stabilized cyclic stress-strain curves for as-cast (black) and forged Mg (red)

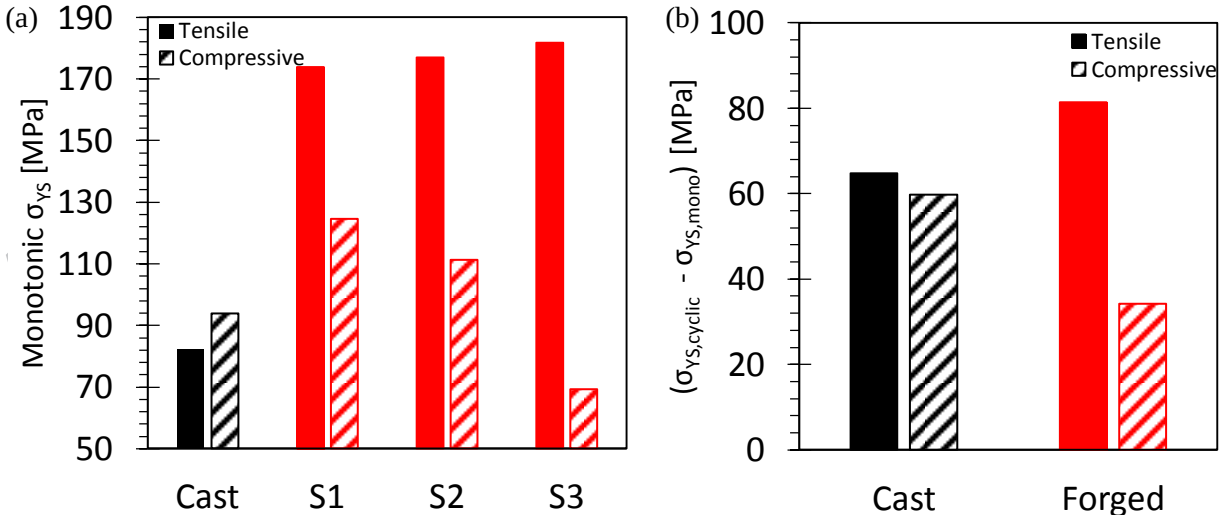

Figure 6 - Summary of (a) monotonic yield strengths and (b) change in yield strengths following cyclic testing for both the as-cast (black) and forged (red) material in tension and compression.

Figure 7 illustrates the hysteresis loops for the first cycle, and stabilized cycles for both the as-cast and forged conditions at a strain amplitude of 0.5%. It can be seen that the peak stresses at the "apex" of both the upward and downward (i.e. reverse loading) reversal are very similar in the cast material (Figure 7 a) for the first and stabilized cycles. The cyclic hardening is also evident from the significant increase in peak stresses from the first cycle to the stabilized cycle; this increase is similar in both tension and compression. The area within the stabilized hysteresis loop represents the dissipated plastic strain energy density, and is calculated to be 0.5 MJ m^{-3} in the case of the cast material at a strain amplitude of 0.5%. In contrast to this, the forged material (Figure 7(b)) exhibits an initial response (first cycle) that is asymmetric, with different curve shapes for the upward and downward reversals, indicative of the occurrence of different deformation mechanisms. The peak stress in compression evolves only marginally as the number of cycles increase, whereas the peak stress in tension increases considerably from the first to the stabilized cycle. This indicates vigorous hardening in tension, and only negligible hardening in compression. In the stabilized cycle the peak stresses in tension are about 77 MPa greater than those in compression, further reinforcing the asymmetric cyclic response of the forged material. As compared with the cast material, the cyclic plastic energy density of the forged material is 0.31 MJ m^{-3} (38% lower), indicative of a more elastic response at a strain amplitude of 0.5%.

Figure 8 illustrates the hysteresis loops for the first and stabilized cycles for the as-cast and forged materials for a high strain amplitude (1.0%). Similar to the observations at a 0.5% strain amplitude, at 1.0% the as-cast material exhibits cyclic hardening with the peak stresses increasing both symmetrically and considerably up to the stabilized cycle, with only a marginal disparity in the peak stress in tension and compression observed in the stabilized cycle. In the forged material, the asymmetric response is even more pronounced at a strain amplitude of 1.0%, with the peak stabilized tensile stress being 114 MPa greater than that observed in the downward reversal. Cyclic hardening is now observed in both tension and compression in the forged material as the peak stresses both evolve over a cumulative number of cycles; however, the hardening is much stronger in tension than in compression. Both materials exhibit significant plasticity at the higher strain amplitude of 1.0%, as the cyclic plastic energy density of the stabilized as-cast and forged responses are 2.0 MJ m^{-3} and 1.55 MJ m^{-3}, respectively. Furthermore, the trends in the level of asymmetry observed in the monotonic response also occurred in the cyclic response of the forged material, but not in the cast material.

The asymmetric cyclic response in textured HCP Mg alloys at higher strain amplitudes have been attributed to detwinning and slip-dominated deformation in tension, and twinning-dominated deformation in compression when loading is in the direction perpendicular to the c-axis [27] [50]–[52]. The downward reversal of such materials is characterized by a lower yield strength (as illustrated in forged conditions in Figure 6(a)) followed by a hardening plateau, which is observed in all forged conditions in this study. The extension twinning deformation process observed in compression is facilitated by a reorientation of the crystal lattice by 86.3° towards the direction of loading [43], subsequently putting a large proportion of unit cells in an orientation that is favourable to detwinning upon reverse loading, as the loading axis is now almost aligned with many of these newly re-oriented unit cells, again activating extension twinning in the successive upward (i.e. forward loading) reversal [53][54][43]. However, this twinning-detwinning process is only slightly reversible in nature and detwinning is typically exhausted prior to the end of the reversed tensile loading. This is accompanied by a sharp increase in hardening rate, and consequently a higher tensile peak stress (relative to compressive peak stress) [27]. The shape of the upward reversal response in all forged conditions (especially in the stabilized cycles) shows strong evidence of this aforementioned behaviour, further supporting the concept of texture-induced asymmetry.

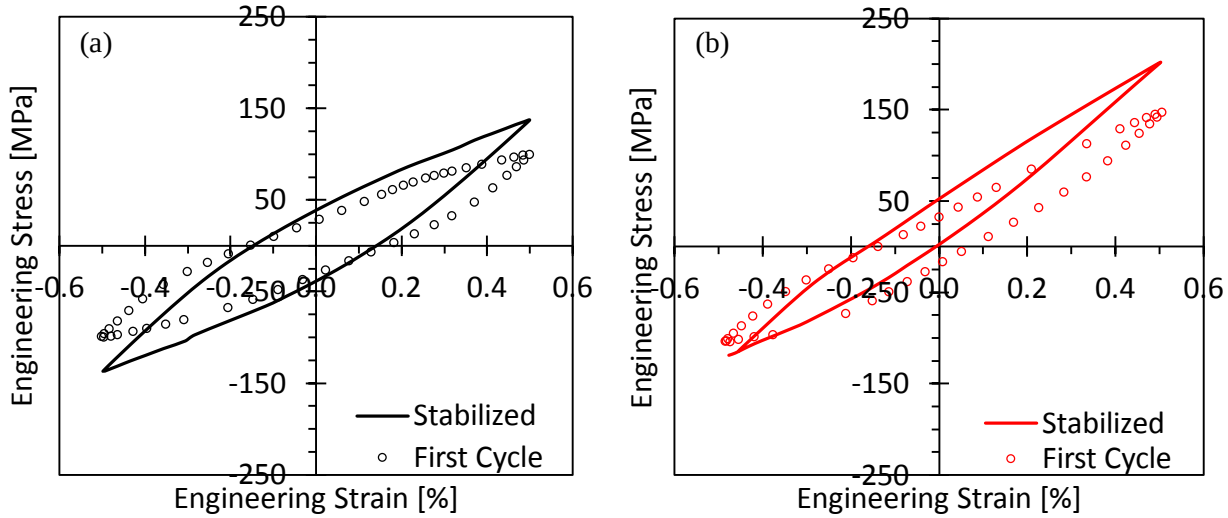

Figure 7 - Axial cyclic behaviour of AZ80 at a strain amplitude of 0.5% in (a) as-cast and (b) forged samples

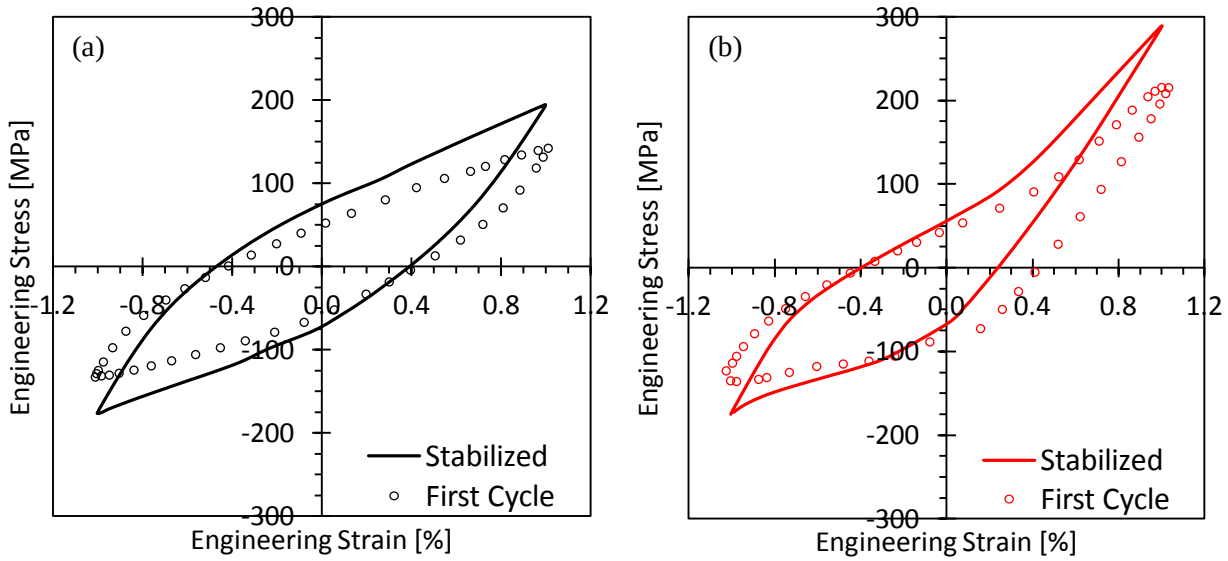

Figure 8 - Axial cyclic behaviour of AZ80 at a strain amplitude of 1.0% (a) as-cast and (b) forged samples

Figure 9 shows the plastic strain response vs. number of cycles throughout the fatigue tests for the as-cast and forged materials at strain amplitudes of 0.5% and 1.0%. As expected, higher strain amplitudes correspond to larger plastic strain components. Furthermore, there is a decrease in maximum plastic strain with number of cycles for both materials and at all strain amplitudes, supporting the cyclic hardening observation discussed earlier. It can be seen that the plastic strain observed in compression is similar between the as-cast and forged materials; the only difference being a higher number of cycles to failure in the forged material. This is due to the similarity in the cyclic yield and flow curve as depicted by Fig. 5b. However, in tension, there is a stark contrast between the plastic strain of the as-cast and forged materials (Figure 9). At a 0.5% strain amplitude, the forged material exhibits 39% less plastic strain than the as-cast material. At a 1.0% strain amplitude, this difference decreases to 25%, but is still considerable, confirming a higher elastic response and higher cyclic yield strength in the forged material. This difference in the plastic strain observed in tension can be directly attributed to the exhaustion of

detwinning in the upward reversal and the associated sudden increase in hardening rate and peak stress, as previously discussed [55].

Figure 10 shows the evolution of mean stress vs number of cycles for various strain amplitudes. For all strain amplitudes of the as-cast material, a negligible amount of mean stress develops. In contrast, in the forged material, a significant amount of mean stress (ranging from 15–55 MPa) develops, with higher mean stresses being typical of larger strain-amplitude fatigue tests. These findings are similar to those discussed earlier (e.g., [27] for AZ31B rolled sheet). The forged material responses are characterized by a fairly consistent increase in mean stress, which reaches a maxima prior to failure. The peak values of mean stress for the forged material are 30, 44, 48, and 57 MPa at strain amplitudes of 0.3%, 0.5%, 0.7%, and 1.0% respectively. The increase in mean stress occurs at a proportion of the total life of the material; this increase ranges from 20–90% depending on the strain amplitude. At low-strain amplitudes (0.3%) the peak mean stress occurs at a cycle count equivalent to 20% of the number of cycles required to cause failure. At higher strain amplitudes (1.0%, Figure 10) a higher proportion of cycles (close to 75%) of the total life is required to reach maximum mean stress

Figure 11 shows the stabilized cyclic response for the (a) as-cast and (b) forged materials at a variety of strain amplitudes. There is apparent symmetry in the as-cast material cyclic response, and hardening behaviour analogous to that observed in the monotonic response (evidence of predominantly slip in tension and weakly mixed-mode hardening (slip and diffuse twinning) in compression). In contrast, the forged material (Figure 11(b)) shows asymmetry with a sigmoidal downward reversal shape and a pronounced shift in hardening behaviour in the upward reversal. This upward reversal response is not observed in monotonic tension as the strain history plays a role in the deformation mechanism, i.e. the first cycle, which starts in tension, shows a response identical to that of the monotonic test. However, the stabilized response has a high propensity to detwin in the upward reversal due to the reorientation of the c-axis resulting from the extension twinning experienced in the previous downward reversal. This phenomenon occurred regardless of forged material condition or strain amplitude, though evidence of it was more pronounced at higher strain amplitudes. The observation that the texture intensification due to forging results in an asymmetric response in both a monotonic and cyclic manner is supported by previous work on other textures, and on material processing methods of various wrought Mg alloys [18], [23], [27], [38], [42], [50], [54], [56], [57].

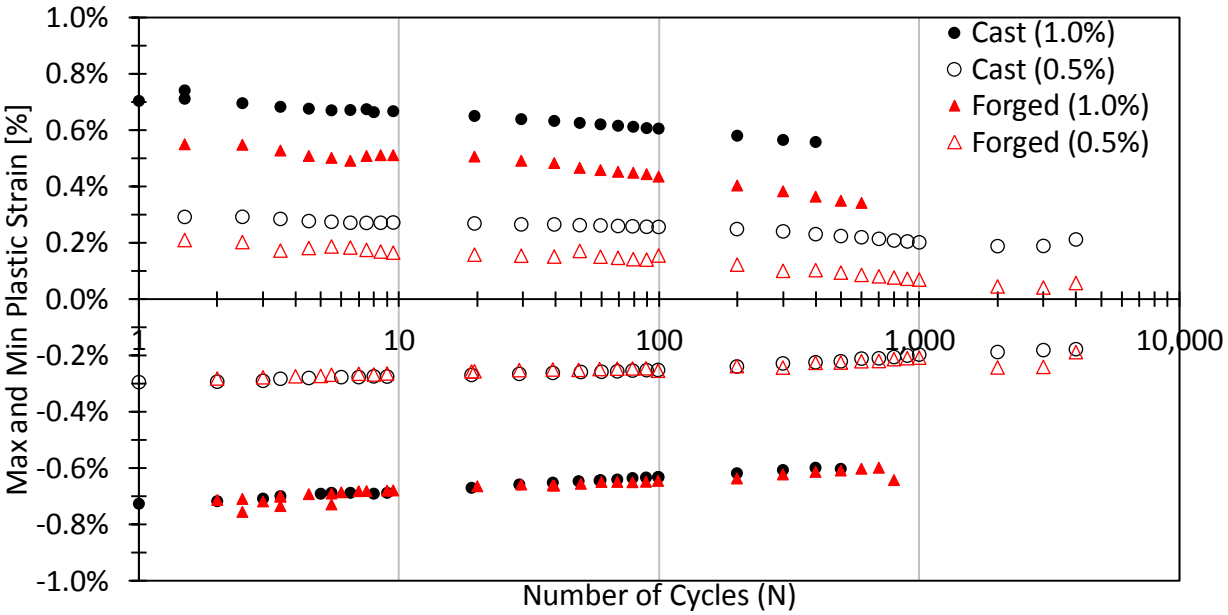

Figure 9 – Plastic strain response during strain-controlled cyclic testing showing variations in peak tensile and compressive plastic strain vs. number of cycles for both as-cast (black) and forged material (red), at 1.0% and 0.5% strain amplitudes

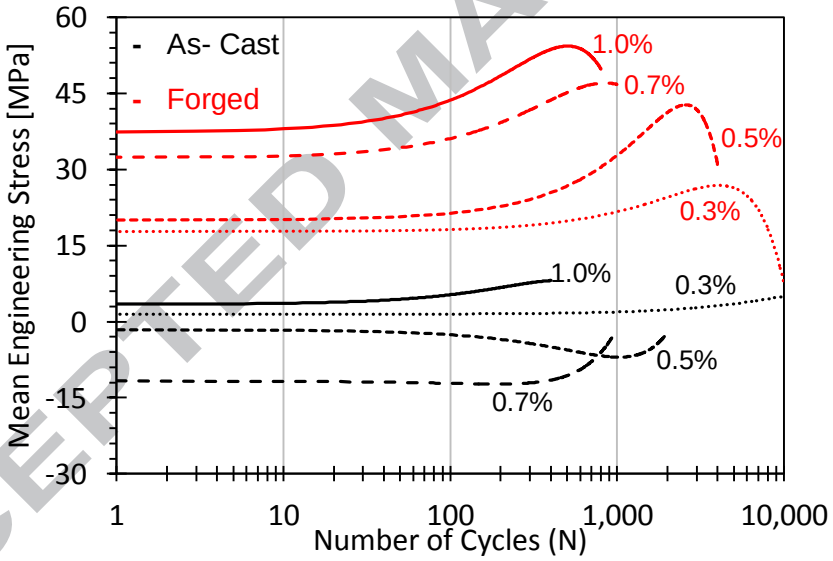

Figure 10 - Stress response during strain-controlled cyclic testing showing variations in mean stress vs. number of cycles at various strain amplitudes (results for 0.3% are only shown up to 10,000 cycles)

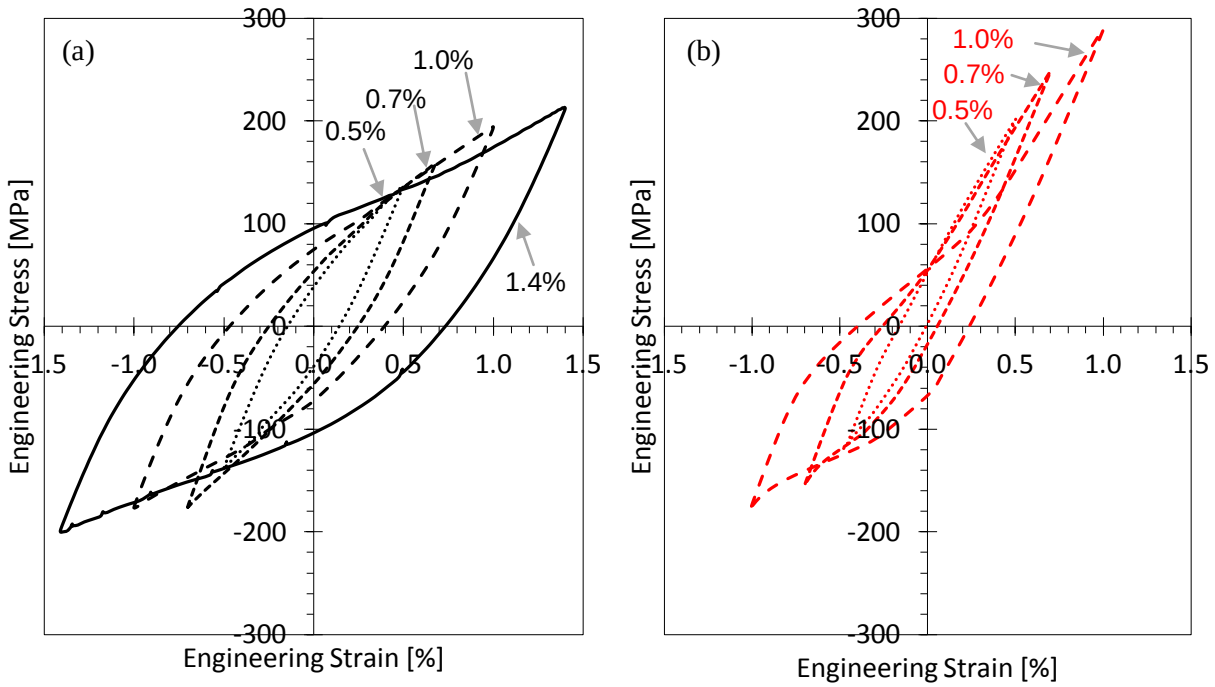

Figure 11 - Stabilized cyclic axial behaviour of (a) as-cast and (b) forged AZ80 Mg alloy

3.3 Fatigue Life

Figure 12 shows the strain-life (ε-N) curve obtained from strain-controlled fatigue testing of the as-cast and forged samples. The data points represent all of the test results, which were conducted on the as-cast and forged material. The dashed lines represent the Coffin-Manson curves for both material types. The forged material has a longer life across all strain amplitudes compared to the cast material. The improvement in life as a result of forging ranges from a factor of approximately 2 times greater in the LCF regime at a 1.4% strain amplitude, to 5 times greater in the HCF regime at a 0.3% strain amplitude. The tests that did not fail after 10^7 cycles are considered to be "run out" and are denoted with an arrow in the figure.

Also shown are the stabilized responses for the as-cast and forged materials at strain amplitudes of 0.3%, 0.7%, and 1.4% plotted on the same axis of engineering stress and strain to facilitate a direct comparison between them. The downward reversal response is similar (in terms of peak stress) between the as-cast and forged materials; however the tensile peak stress in each hysteresis loop is much greater in the forged material. It is well known that a tensile mean stress, as exhibited by the forged materials in this study, has a detrimental effect on fatigue life [12]. This implies that the forged material would exhibit a shorter life because of the presence of positive mean stress. However, the plastic energy density or cyclic energy (area inside the hysteresis loop) is also considerably lower in the forged material for all strain amplitudes, indicative of a lesser extent of incurred damage per cycle and a corresponding increase in fatigue life.

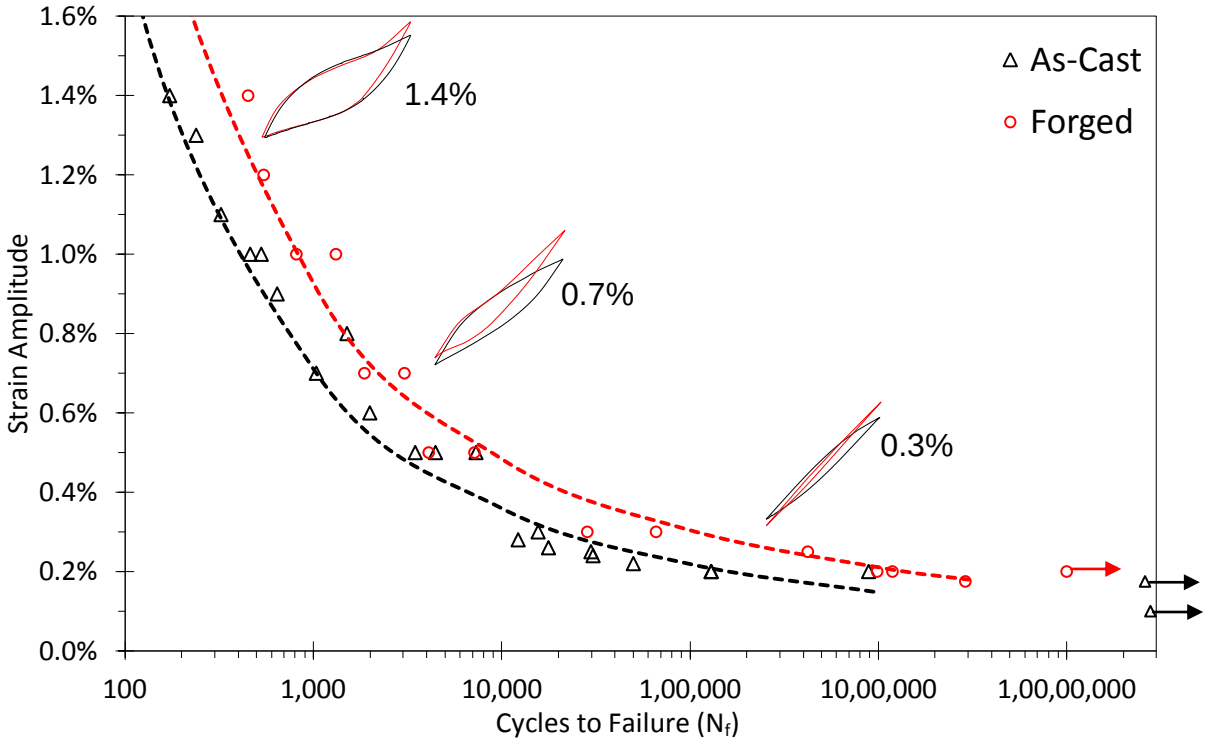

Figure 12 – ε-N curves for as-cast (black) and forged (red) AZ80 Mg alloy obtained at strain amplitudes between 0.1 and 1.4%

3.4 Fracture Mechanisms

Scanning Electron Microscope images showing the macroscopic features of the fracture surface of the fatigue specimens are shown in Figure 13(a) and (c). All samples exhibited fatigue crack initiation (FCI) at the specimen surface. The as-cast material (Figure 13(a)) exhibits a fracture surface with a faceted morphology, substantial cleavage-like terraces, and widespread macroscopic striations of varying orientations. These distinct features show evidence of mixed deformation dominated by slip over a large portion of the area. The random facet orientation is indicative of varying crystal orientations associated with the randomized texture of the as-cast material. Terrace edges appear to correspond with grain boundaries, as they demark thresholds of varying macro-striation orientations. The propagation zone is also comparatively rough relative to the forged sample (Figure 13c). In contrast, the forged sample exhibited a distinct FCI with radially branching beach marks and a large propagation zone, which is much flatter and more stable than the as-cast condition. The final fracture zone is located opposite to the FCI location, indicating stable crack propagation in a direction approximately perpendicular to the initial fatigue crack propagation direction, as is typical with R= −1 strain-controlled fatigue testing. Guo et al. [15] investigated the fracture behaviour of cast-homogenized AZ80 Mg alloy that was processed via multi-directional forging. They observed that cracks initiated at the brittle $Mg_{17}Al_{12}$ particles, and then propagated and coalesced along grain boundaries [15]. Crack initiation tends to occur at the brittle second phase particles in AZ80 Mg alloy [18][10][5]. The presence of dimpled final fracture surface morphology is the main characteristic differentiating the forged from the as-cast conditions. The depth of the dimples is an indicator of ductility, with deeper dimples occurring as a result of more plasticity. Xiong et al. [18] observed that dimple-like features were evident in the final fracture region of rolled AZ80 fatigue specimens, tested in a direction perpendicular to the c-axis(the LD orientation of fatigue samples in the forgings presented here is also orthogonal to the c-axis). This agrees well with the more ductile tensile

monotonic response of the material following forging. The final fracture zone surface morphology is shown in Figure 13 (b) and (d). The as-cast material (b) shows some evidence of ductility, as well as dendrite tear-out morphology with a faceted structure. The forged sample (d) showed more evidence of ductility, including a surface morphology with pronounced dimpling, and a terrace-like structure supporting the observation of more plastic fracture behaviour.

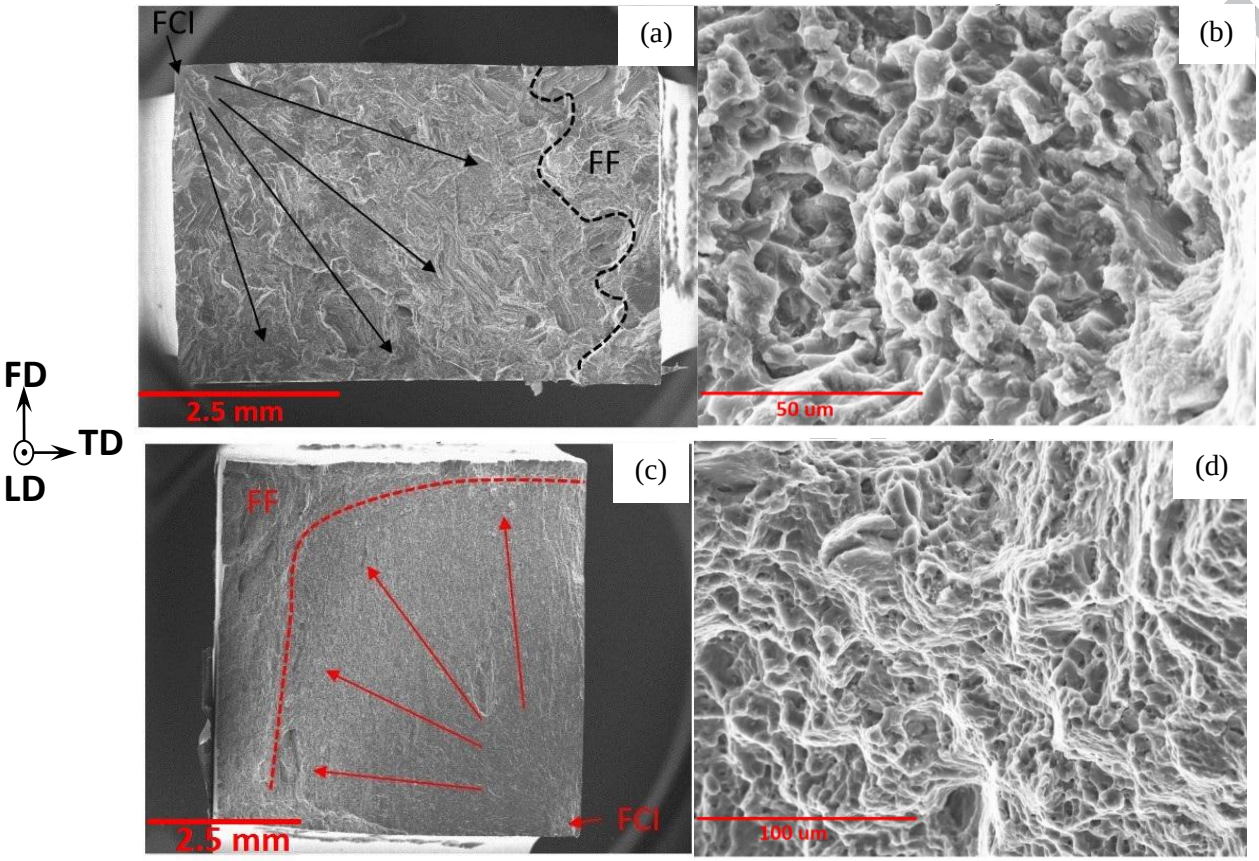

Figure 13 - Fracture surfaces of the as-cast ((a) and (b)) and forged conditions ((c) and (d)) for samples tested at a strain amplitude of +/- 0.3%. As-cast sample fractured at 15, 644 cycles and forged sample at 66, 171 cycles. FCI denotes the fatigue crack initiation location and arrows denote the approximate propagation direction. Images (b) and (d) show a detailed view of the surface morphology in the final fracture (FF) zone.

3.5 Fatigue Life Modelling

To quantitatively compare the damage incurred during cyclic loading in wrought Mg, numerous fatigue damage parameters, including stress, strain and energy-based parameters, have been proposed [42][56]. As exhibited in Figure 4, some forms of AZ80 may display perfectly plastic cyclic behaviour, post cyclic yield, or even cyclic softening, since within an arbitrary range of applied strain amplitudes, the stress may remain constant or may decrease. While successful attempts have been made to model fatigue life of Mg alloys using stress-based damage model (e.g., [58]for hot-rolled AZ31B) , in general stress-based fatigue models are not ideal as they cannot accurately capture fatigue damage inflicted under these ranges of deformation conditions. The objective of the following is to investigate the suitability and accuracy of existing strain and energy based models at predicting the fatigue life of AZ80 as-cast and forged material. The strain-based critical plane SWT model and energy based Jahed-Varvani models are examined here.

3.5.1 Smith-Watson-Topper: SWT Model

The SWT parameter [59] was initially formulated to account for the mean stress effect during fatigue loading. Modified versions of this model have been extended for use in multiaxial life predictions of Mg alloys using a critical plane method with good success [60]. The SWT parameter is related to fatigue life in terms of four different material constants:

$$\sigma_{n,max}\frac{\Delta\varepsilon_1}{2} = \frac{{\sigma'_f}^2}{E}(2N_f)^{2n} + \sigma'_f\varepsilon'_f(2N_f)^{b+c}$$

The term $\Delta\varepsilon_1$ represents the principal strain range, $\sigma_{n,max}$ represents the maximum stress on the plane of principal strain, and E, the modulus of elasticity (in the case of Mg E=44 GPa). The Coffin-Manson constants on the right hand side of the equation were extracted from strain-controlled test results, as shown in Figure 14(a) and (b), and are summarized in Table 2. The symbols shown represent the experimental data extracted from the stabilized hysteresis loops for both the as-cast and forged material, and the dashed lines represent a fit to the elastic and plastic parts of strain. The elastic part of the strain range was calculated from $\Delta\varepsilon^e = \Delta\sigma/E$, and the plastic strain range was obtained from $\Delta\varepsilon^p = \Delta\varepsilon - \Delta\varepsilon^e$. Figure 14(c) shows the calculated SWT parameter for both the as-cast and forged material fatigue data as a function of cycles to failure. Both the as-cast and forged materials can be expressed using power-law fits, albeit with unique constants for each material. This implies that the SWT damage parameter for the forged material is higher than that of the cast material. This is expected as the maximum normal stress is higher in the tensile peak of the stabilized response in the forged material than in the cast material at an equivalent strain amplitude. Using the parameters given in Table 2, the fatigue life was predicted for both the as-cast and forged materials, and is plotted versus the experimental life in Figure 14(d). The solid diagonal line denotes a correlation match between the predicted and experimental life, and the dashed lines represent bounds that envelop deviation from this match by a factor of 2. The vast majority of life estimations fall within these bounds of a factor of 2, with almost equal numbers of data being under and over predicted. For both the as-cast and forged materials, the LCF regime seems to be conservative in its prediction, and trends towards slightly non-conservative in the HCF regime. One of the reasons for conservative predictions in the LCF regime is that the stabilized responses are used as model inputs, and for materials that cyclically harden, the stabilized cycles are more damaging than the initial ones (as the peak stresses are higher). Since the "transient" phase of hardening is a non-negligible portion of the life for the LCF regime, a proportion of the cycles experienced by the experimental samples undergo slightly less damage than predicted, as their peak stresses are lower. This is, however, a minor discrepancy and the assumption that the stabilized response is used is widely accepted in the literature. The coefficient of determination is $R^2 = 0.94$ for the as-cast prediction, and $R^2 = 0.98$ for the forged material prediction.

Table 2 - Coffin-Manson parameters for SWT model for cast and forged AZ80 Mg

ID	σ'_f (MPa)	b	ε'_f	c
As-Cast	479.6	-0.141	0.2714	-0.577
Forged	598.4	-0.131	0.3395	-0.576

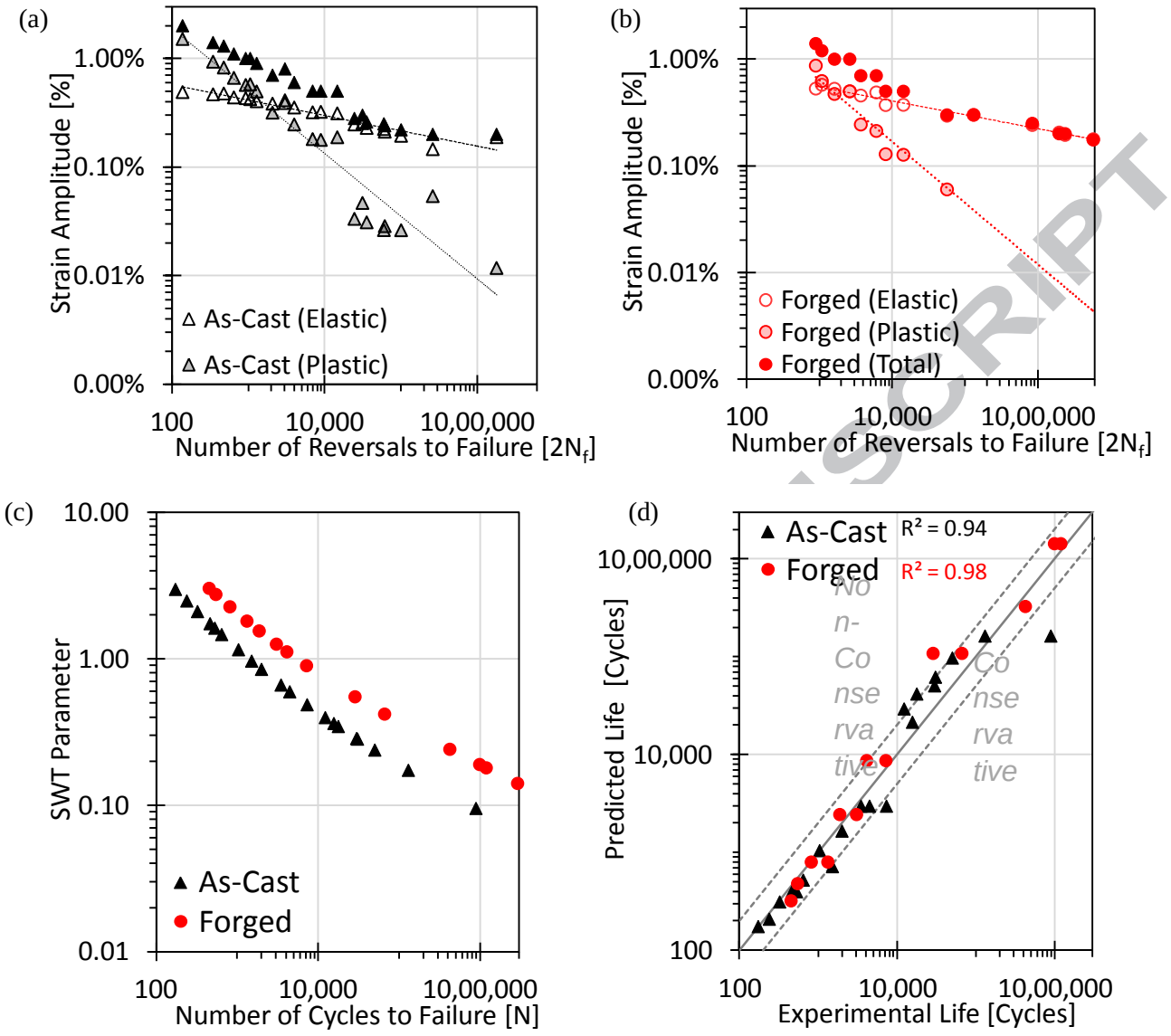

Figure 14 - Strain-life data used for extracting Coffin-Manson constants in (a) as-cast and (b) forged AZ80 Mg; (c) SWT damage parameter evolution with number of cycles to failure for both as-cast and forged AZ80 Mg; and (d) the correlation between SWT-predicted fatigue life and experimental life for both as-cast and forged AZ80 Mg

3.5.2 Jahed-Varvani – JV Energy-based Model

Energy-based fatigue damage models have been used by many researchers for modeling the fatigue life of Mg alloys, e.g., Park et al. [27][61] in rolled AZ31, Xiong et al. [18] for rolled AZ80, Jahed et al. [62] for many different Mg alloys and conditions, and Albinmousa et al. [63] for AZ31 under multiaxial loading to predict the fatigue life of wrought Mg alloys. In this study, the JV model [64] is utilized. The significance of this life model is in the evaluation of the fatigue material constants from energy-life curve. In this model, the total energy density is implemented as a damage parameter and is constituted by its elastic and plastic components. The plastic component is defined as the area enveloped by the stabilized hysteresis loop and the elastic component is defined as the following equation[65]:

$$\Delta E_e{}^{+} = \frac{{\sigma_{max}}^2}{2E}$$

where σ_{max} is the peak tensile stress. Adding the positive elastic strain energy density, the mean stress effect is also taken into account in this model [65] and subsequently the energy damage parameter ΔE is related to fatigue life via an analogues equation of similar form to the Coffin-Manson equation. [64][66], where ΔE is the strain energy density:

$$\Delta E = E_e{}'(2N_f)^B + E_f{}'(2N_f)^C$$

Coefficient $E_f{}'$ correspond to the fatigue toughness and $E_e{}'$ is the fatigue strength coefficient. Exponents *C* and *B* are the fatigue toughness and fatigue strength exponents, respectively. The constants in the above equation are extracted from the strain energy density life curves presented in Figure 15 for the as-cast and forged materials, and those parameters are summarized below in Table 3. The same fatigue data extracted from the set of tests performed in this study used in the strain-based prediction results in Figure 14 are used in calculation of these energy-based model parameters. The symbols in Figure 15(a) and (b) represent this aforementioned fatigue data, and the dashed lines represent the fits to elastic and plastic portions of the energy density. Figure 15(c) shows the calculated energy damage parameter for both the as-cast and forged material fatigue data as a function of cycles to failure. Both the as-cast and forged materials can be expressed using very similar curves, as the data points almost consolidate onto one single curve. This can be attributed to the competing effect forging has on the magnitude of elastic and plastic components of the damage parameter. For a given strain amplitude, the forged material has a higher tensile peak stress causing the elastic energy to be higher, and less enveloped within the stabilized hysteresis loop area, resulting in less plastic energy. As a result, the total energy remains almost unchanged for a given life in both as-cast and forged materials.

Using the parameters in Table 3, the fatigue life was predicted for both the as-cast and forged materials, and is plotted versus the experimental life in Figure 15(d). Almost all the life estimations fall within these bounds of a factor of 2, with almost equal numbers of data being under and over predicted. The coefficient of determination is R^2 = 0.95 for the as-cast prediction, and R^2 = 0.99 for the forged material prediction.

Table 3 - Energy-based parameters for the Jahed-Varvani model for cast and forged AZ80 Mg

ID	$E_e{}'$ (MJ/m^3)	$E_f{}'$ (MJ/m^3)	*B*	C
Cast	3.5861	68.39	-0.309	-0.555
Forged	7.9094	758.6	-0.304	-0.836

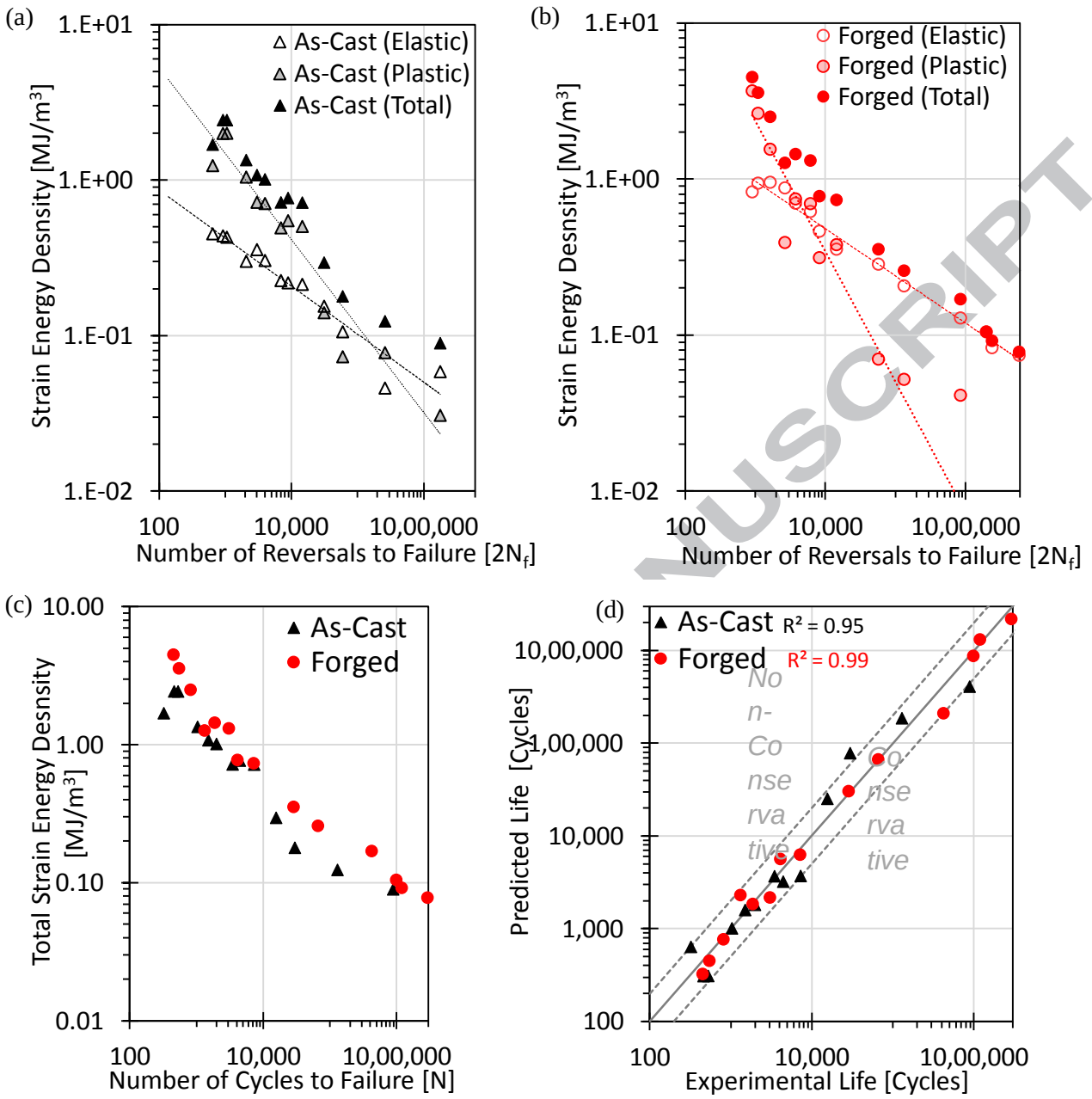

Figure 15 – Strain energy-life data used for extracting energy-based constants in (a) as-cast and (b) forged AZ80 Mg; (c) Jahed-Varvani damage parameter evolution with number of cycles to failure for both as-cast and forged AZ80 Mg; and (d) the correlation between the Jahed-Varvani predicted fatigue life and experimental life for both as-cast and forged AZ80 Mg

4. Conclusions

Uniaxial quasi-static and fully-reversed fatigue experiments were conducted at various strain amplitudes, ranging from 0.1–1.4% of both as-cast and forged AZ80 Mg alloy. The effects of various forging parameters (temperature and deformation rate) on the quasi-static properties were investigated on a comparative basis. Based on the results the following conclusions can be drawn:

1. Microstructural analysis showed that AZ80 Mg alloy in the as-cast condition possessed a microstructure consisting of primarily α-phase and aluminium-rich β-phase, while the forged material showed a recrystallized microstructure, with smaller, equiaxed grains. The as-cast material showed a random texture, leading to nearly symmetric properties invariant of material direction. The thermomechanical history imparted to the material via forging resulted in a texture intensification and a rotation of the crystallographic cells to align with the loading direction during forging.

2. Texture intensification due to forging results in tension-compression asymmetry in both the monotonic and cyclic responses. The forged material exhibited substantial increases in strength and ductility, especially in tension, with the benefit of compressive properties being somewhat masked by the twinning deformation mode, which requires lower stress to be activated and becomes prevalent following texture intensification. The monotonic tensile tests showed that AZ80 in the forged condition had considerably higher ultimate strength and ductility relative to the as-cast alloy. After forging of as-cast AZ80, increases in ultimate tensile strength from 234 MPa to 312 MPa in tension, and from 318 MPa to 373 MPa in compression were observed. The fracture strain increased from 8.5% to 15.8% in tension, and decreased from 15.3% to 9.6% in compression after forging.

3. The cyclic responses of AZ80 differed significantly between the as-cast and forged material. The shapes of the stabilized hysteresis loops of all the forged conditions varied from that of the as-cast material, with differences being especially marked in the tensile regime, with pronounced tensile tips and higher peak stresses, in the forged material. The unique characteristics of the cyclic response are governed by key differences in the mechanisms that control deformation. At strain amplitudes at which appreciable plasticity occurs, the as-cast material exhibits predominantly slip deformation in the upward reversal, and marginally mixed-mode in the downward reversal. In contrast, the forged material exhibits twinning in the downward reversal and detwinning, followed by slip, in the upward reversal, regardless of the forging condition. This unique characteristic of the cyclic deformation mechanism in the forged material is the primary source of the observed asymmetric response.

5. Once forged, the AZ80 Mg alloy exhibits superior fatigue properties relative to the as-cast material under strain-controlled testing over the entire strain range investigated in this study. The improvement in fatigue life as a result of forging ranges from 2 times greater in the LCF regime, to 5 times greater in the HCF regime. This improvement was observed in the forged material despite the development of significant tensile mean stress.

6. The fracture surfaces of as-cast samples were characterized by a terrace-like faceted morphology, whereas the forged conditions exhibited a more dimple-like fracture surface, indicative of greater plasticity.

7. The JV energy-based model and SWT critical plane model give reliable fatigue life predictions for as-cast and forged AZ80.

Acknowledgements

The financial support of the Natural Sciences and Engineering Research Council of Canada (NSERC) through the Automotive Partnership Canada (APC) under APCPJ 459269–13 grant with contributions from Multimatic Technical Centre, Ford Motor Company, and Centerline Windsor are acknowledged. The authors would also like to acknowledge J. McKinley from CanmetMATERIALS, Hamilton for forging trials.

References

[1] J. Pan, "Sound Package Design for Lightweight Vehicles," *SAE Int.*, no. 10.4271/2015-01-2343, 2015.

[2] Q. Guo, H. G. Yan, Z. H. Chen, and H. Zhang, "Grain refinement in as-cast AZ80 Mg alloy under large strain deformation," *Mater. Charact.*, vol. 58, no. 2, pp. 162–167, 2007.

[3] P. Zhang and J. Lindemann, "Influence of shot peening on high cycle fatigue properties of the high-strength wrought magnesium alloy AZ80," *Scr. Mater.*, vol. 52, no. 6, pp. 485–490, 2005.

[4] P. Moldovan, G. Popescu, D. Bojin, D. Constantinescu, and M. Pana, "Improving the fatigue resistance of magnesium alloys for forged parts in automotive industry," *Metal. Int.*, vol. 14, no. SPEC. ISS. 2, pp. 23–26, 2009.

[5] Y. Uematsu, K. Tokaji, and M. Matsumoto, "Effect of aging treatment on fatigue behaviour in extruded AZ61 and AZ80 magnesium alloys," *Mater. Sci. Eng. A*, vol. 517, no. 1–2, pp. 138–145, 2009.

[6] G. Kurz, B. Clauw, W. H. Sillekens, D. Letzig, and P. Manufacturing, "Die Forging of the Alloys Az80 and Zk60," *Mater. Soc. Annu. Meet.*, pp. 197–202, 2009.

[7] P. Moldovan and D. M. Constantinescu, "Magnesium Alloys for Automotive Applications," *Metal. Int.*, vol. 14, no. 7, pp. 19–23, 2009.

[8] F. Nový, M. Janeček, V. Škorik, J. Muller, and L. Wagner, "Very high cycle fatigue behaviour of as-extruded AZ31, AZ80, and ZK60 magnesium alloys," *Int. J. Mater. Res.*, vol. 100, no. 3, pp. 288–291, 2009.

[9] K. Shiozawa, T. Kashiwagi, T. Murai, and T. Takahashi, "Fatigue behaviour and fractography of extruded AZ80 magnesium alloys in very high cycle regime," *Procedia Eng.*, vol. 2, no. 1, pp. 183–191, 2010.

[10] M. S. Bhuiyan, Y. Mutoh, T. Murai, and S. Iwakami, "Corrosion fatigue behavior of extruded magnesium alloy AZ80-T5 in a 5% NaCl environment," *Eng. Fract. Mech.*, vol. 77, no. 10, pp. 1567–1576, 2010.

[11] P. Zhang, J. Lindemann, and C. Leyens, "Shot peening on the high-strength wrought magnesium alloy AZ80-Effect of peening media," *J. Mater. Process. Technol.*, vol. 210, no. 3, pp. 445–450, 2010.

[12] K. Shiozawa, J. Kitajima, T. Kaminashi, T. Murai, and T. Takahashi, "Low-cycle fatigue deformation behavior and evaluation of fatigue life on extruded magnesium alloys," *Procedia Eng.*, vol. 10, pp. 1244–1249, 2011.

[13] R. Zhu, W. Ji, Y. Wu, X. Cai, and Y. Yu, "Effect of aging treatment on low-cycle fatigue behavior of extruded Mg-8Al-0.5Zn alloys," *Mater. Des.*, vol. 41, pp. 203–207, 2012.

[14] R. Liu, D. L. Yin, and J. T. Wang, "Elimination of yielding asymmetry in extruded AZ80 alloy by ageing," *Trans. Nonferrous Met. Soc. China (English Ed.)*, vol. 24, no. 4, pp. 915–921, 2014.

[15] Q. Guo, H. G. Yan, Z. H. Chen, and H. Zhang, "Fracture behaviors of AZ80 magnesium alloy during multiple forging processes," *Trans. Nonferrous Met. Soc. China (English Ed.)*, vol. 16, no. 4, pp. 922–926, 2006.

[16] H. T. Zhou, Q. B. Li, Z. K. Zhao, Z. C. Liu, S. F. Wen, and Q. D. Wang, "Hot workability characteristics of magnesium alloy AZ80-A study using processing map," *Mater. Sci. Eng. A*, vol. 527, no. 7–8, pp. 2022–2026, 2010.

[17] G. Z. Quan, T. Song, Y. J. Zhou, F. B. Wang, and J. Zhou, "Relationship between mechanical properties and grain size of AZ80 at 350 °c under different strain rates," *Trans. Nonferrous Met. Soc. China (English Ed.)*, vol. 20, no. SUPPL. 2, pp. 0–4, 2010.

[18] Y. Xiong and Y. Jiang, "Cyclic deformation and fatigue of rolled AZ80 magnesium alloy along different material orientations," *Mater. Sci. Eng. A*, vol. 667, pp. 58–67, 2016.

[19] P. Zhang and J. Lindemann, "Effect of roller burnishing on the high cycle fatigue performance of the high-strength wrought magnesium alloy AZ80," *Scr. Mater.*, vol. 52, no. 10, pp. 1011–1015, 2005.

[20] G. Rivers, "Cyclic Fatigue Testing of Wrought Magnesium AZ80 Alloy for Automotive Wheels,", McMaster University, 2009.

[21] H. Okada, Y. Uematsu, and K. Tokaji, "Fatigue behaviour in AZ80A magnesium alloy with DLC/thermally splayed WC-12Co hybrid coating," *Procedia Eng.*, vol. 2, no. 1, pp. 283–290, 2010.

[22] G. Rivers, "Cyclic Fatigue Behaviour of Wrought AZ80 Magnesium Alloy from Forged Automotive Wheel," McMaster University, 2011.

[23] C. Wang, T. Luo, and Y. Yang, "Low cycle fatigue behavior of the extruded AZ80 magnesium alloy under different strain amplitudes and strain rates," *J. Magnes. Alloy.*, vol. 4, no. 3, pp. 181–187, 2016.

[24] R. C. Zeng, Y. B. Xu, W. Ke, and E. H. Han, "Fatigue crack propagation behavior of an as-extruded magnesium alloy AZ80," *Mater. Sci. Eng. A*, vol. 509, no. 1–2, pp. 1–7, 2009.

[25] R. Zeng, E. Han, and W. Ke, "A critical discussion on influence of loading frequency on fatigue crack propagation behavior for extruded Mg-Al-Zn alloys," *Int. J. Fatigue*, vol. 36, no. 1, pp. 40–46, 2012.

[26] Y. Lou, L. Li, J. Zhou, and L. Na, "Deformation behavior of Mg-8Al magnesium alloy compressed at medium and high temperatures," *Mater. Charact.*, vol. 62, no. 3, pp. 346–353, 2011.

[27] S. Hyuk Park, S. G. Hong, B. Ho Lee, W. Bang, and C. Soo Lee, "Low-cycle fatigue characteristics of rolled Mg-3Al-1Zn alloy," *Int. J. Fatigue*, vol. 32, no. 11, pp. 1835–1842, 2010.

[28] D. Kobold, T. Pepelnjak, G. Gantar, and K. Kuzman, "Analysis of deformation characteristics of magnesium AZ80 wrought alloy under hot conditions," *Stroj. Vestnik/Journal Mech. Eng.*, vol. 56, no. 12, pp. 823–832, 2010.

[29] H. Z. Li, X. Y. Wei, J. Ouyang, J. Jiang, and Y. Li, "Hot deformation behavior of extruded AZ80 magnesium alloy," *Trans. Nonferrous Met. Soc. China (English Ed.)*, vol. 23, no. 11, pp. 3180–3185, 2013.

[30] Z. Su, L. Wan, C. Sun, Y. Cai, and D. Yang, "Hot deformation behavior of AZ80 magnesium alloy towards optimization of its hot workability," *Mater. Charact.*, vol. 122, pp. 90–97, 2016.

[31] L. Wang *et al.*, "Effects of texture and grain size on mechanical properties of AZ80 magnesium alloys at lower temperatures," *Mater. Des.*, vol. 89, pp. 1–8, 2016.

[32] J. Yoon and J. Lee, "Process design of Warm-Forging with extruded Mg-8Al-0.5Zn alloy for differential case in automobile transmission," *Int. J. Precis. Eng. Manuf.*, vol. 16, no. 4, pp. 841–846, 2015.

[33] M. Madaj, M. Greger, and V. Karas, "Magnesium-alloy die forgings for automotive applications," *Mater. Tehnol.*, vol. 49, no. 2, pp. 267–273, 2015.

[34] A. Gontarz and A. Dziubińska, "Forming of flat parts with ribs from magnesium alloy," *Aircr. Eng. Aerosp. Technol.*, vol. 86, no. 4, pp. 356–360, 2014.

[35] M. engineering Yoon, Jonghun; Hanyang University, "Warm-Forging of AZ80 Magnesium Alloy for Control-Arm in Automobile," *J.*

Automob. Eng., no. 434, pp. 1–36, 2012.
[36] Q. Wang, Z. M. Zhang, X. Zhang, and J. M. Yu, "Precision forging technologies for magnesium alloy bracket and wheel," *Trans. Nonferrous Met. Soc. China (English Ed.)*, vol. 18, no. SPEC. ISSUE 1, pp. s205–s208, 2008.
[37] V. Kevorkijan, "AZ80 and ZC71/SiC/12p closed die forgings for automotive applications: technical and economic assessment of possible mass production," *Materials science and technology*, vol. 19, no. 10. pp. 1386–1390, 2003.
[38] A. A. Roostaei and H. Jahed, "Role of loading direction on cyclic behaviour characteristics of AM30 extrusion and its fatigue damage modelling," *Mater. Sci. Eng. A*, vol. 670, pp. 26–40, 2016.
[39] W. J. Lai, Y. Y. Li, Y. F. Hsu, S. Trong, and W. H. Wang, "Aging behaviour and precipitate morphologies in Mg-7.7Al-0.5Zn-0.3Mn (wt.%) alloy," *J. Alloys Compd.*, vol. 476, no. 1–2, pp. 118–124, 2009.
[40] D. Sarker and D. L. Chen, "Texture transformation in an extruded magnesium alloy under pressure," *Mater. Sci. Eng. A*, vol. 582, pp. 63–67, 2013.
[41] D. Sarker, J. Friedman, and D. L. Chen, "Influence of pre-strain on de-twinning activity in an extruded AM30 magnesium alloy," *Mater. Sci. Eng. A*, vol. 605, pp. 73–79, 2014.
[42] J. Albinmousa and H. Jahed, "Multiaxial effects on LCF behaviour and fatigue failure of AZ31B magnesium extrusion," *Int. J. Fatigue*, vol. 67, pp. 103–116, 2014.
[43] J. M. A. Gryguc, S.K. Shaha, H. Jahed, M. Wells, B. Williams, "Tensile and fatigue behaviour of as-forged AZ31B extrusion," *Multiaxial Fatigue Fract.*, vol. 38, no. 38, pp. 251–258, 2016.
[44] B. Wang, R. Xin, G. Huang, and Q. Liu, "Effect of crystal orientation on the mechanical properties and strain hardening behavior of magnesium alloy AZ31 during uniaxial compression," *Mater. Sci. Eng. A*, vol. 534, pp. 588–593, 2012.
[45] J. Li, J. Liu, and Z. Cui, "Microstructures and mechanical properties of AZ61 magnesium alloy after isothermal multidirectional forging with increasing strain rate," *Mater. Sci. Eng. A*, vol. 643, pp. 32–36, 2015.
[46] L. Liu and H. Ding, "Study of the plastic flow behaviors of AZ91 magnesium alloy during thermomechanical processes," *J. Alloys Compd.*, vol. 484, no. 1–2, pp. 949–956, 2009.
[47] A. Gryguc, H. Jahed, B. Williams, and J. McKinley, "Magforge – Mechanical behaviour of forged AZ31B extruded magnesium in monotonic compression," *Mater. Sci. Forum*, vol. 828–829, pp. 291–297, 2015.
[48] S. Xu, V. Y. Gertsman, J. Li, J. P. Thomson, and M. Sahoo, "Role of Mechanical Twinning in Tensile Compressive Yield Asymmetry of Die Cast Mg Alloys," *Can. J. Metall. Mater. Sci.*, vol. 44, no. 2, pp. 155–165, 2005.
[49] D. Sarker and D. L. Chen, "Detwinning and strain hardening of an extruded magnesium alloy during compression," *Scr. Mater.*, vol. 67, no. 2, pp. 165–168, 2012.
[50] J. Albinmousa, H. Jahed, and S. Lambert, "Cyclic behaviour of wrought magnesium alloy under multiaxial load," *Int. J. Fatigue*, vol. 33, no. 8, pp. 1127–1139, 2011.
[51] A. Staroselsky and L. Anand, "A constitutive model for hcp materials deforming by slip and twinning: Application to magnesium alloy AZ31B," *Int. J. Plast.*, vol. 19, no. 10, pp. 1843–1864, 2003.
[52] L. Wu *et al.*, "Twinning-detwinning behavior during the strain-controlled low-cycle fatigue testing of a wrought magnesium alloy, ZK60A," *Acta Mater.*, vol. 56, no. 4, pp. 688–695, 2008.
[53] S. Kleiner and P. J. Uggowitzer, "Mechanical anisotropy of extruded Mg-6% Al-1% Zn alloy," *Mater. Sci. Eng. A*, vol. 379, no. 1–2, pp. 258–263, 2004.
[54] X. Y. Lou, M. Li, R. K. Boger, S. R. Agnew, and R. H. Wagoner, "Hardening evolution of AZ31B Mg sheet," *Int. J. Plast.*, vol. 23, no. 1, pp. 44–86, 2007.
[55] J. Albinmousa, H. Jahed, and S. Lambert, "Cyclic axial and cyclic torsional behaviour of extruded AZ31B magnesium alloy," *Int. J. Fatigue*, vol. 33, no. 11, pp. 1403–1416, 2011.
[56] E. Kalatehmollaei, H. Mahmoudi-Asl, and H. Jahed, "An asymmetric elastic-plastic analysis of the load-controlled rotating bending test and its application in the fatigue life estimation of wrought magnesium AZ31B," *Int. J. Fatigue*, vol. 64, pp. 33–41, 2014.
[57] Y. Chino, K. Kimura, M. Hakamada, and M. Mabuchi, "Mechanical anisotropy due to twinning in an extruded AZ31 Mg alloy," *Mater. Sci. Eng. A*, vol. 485, no. 1–2, pp. 311–317, 2008.
[58] Y. C. Lin, Z. H. Liu, X. M. Chen, and J. Chen, "Stress-based fatigue life prediction models for AZ31B magnesium alloy under single-step and multi-step asymmetric stress-controlled cyclic loadings," *Comput. Mater. Sci.*, vol. 73, pp. 128–138, 2013.
[59] R. N. Smith, P. Watson, and T. H. Topper, "A Stress-Strain Function for the Fatigue of Metals," *J. Mater.*, vol. 5, no. 4, pp. 767–788, 1970.
[60] D. Scoie, "Multiaxial Fatigue Damage Models," *J. Eng. Mater. Technol.*, vol. 109, no. OCTOBER, pp. 293–298, 1987.
[61] S. H. Park, S. G. Hong, W. Bang, and C. S. Lee, "Effect of anisotropy on the low-cycle fatigue behavior of rolled AZ31 magnesium alloy," *Mater. Sci. Eng. A*, vol. 527, no. 3, pp. 417–423, 2010.
[62] H. Jahed and J. Albinmousa, "Multiaxial behaviour of wrought magnesium alloys - A review and suitability of energy-based fatigue life model," *Theor. Appl. Fract. Mech.*, vol. 73, pp. 97–108, 2014.
[63] J. Albinmousa, H. Jahed, and S. Lambert, "An Energy-Based Fatigue Model for Wrought Magnesium Alloy under Multiaxial Load," *Ninth Int. Conf. Multiaxial Fatigue Fract.*, pp. 471–478, 2010.
[64] H. Jahed and A. Varvani-Farahani, "Upper and lower fatigue life limits model using energy-based fatigue properties," *Int. J. Fatigue*, vol. 28, no. 5–6, pp. 467–473, 2006.
[65] K. Golos and F. Ellyin, "A Total Strain Energy Density Theory for Cumulative Fatigue Damage," *J. Press. Vessel Technol.*, vol. 110, pp. 36–41, 1988.
[66] H. Jahed, A. Varvani-Farahani, M. Noban, and I. Khalaji, "An energy-based fatigue life assessment model for various metallic materials under proportional and non-proportional loading conditions," *Int. J. Fatigue*, vol. 29, no. 4, pp. 647–655, 2007.